

Towards Topological Protection based millimetre wave devices

Gian Guido Gentili,¹ Giuseppe Pelosi,² Francesco S. Piccioli,^{1,3,*} and Stefano Selleri²

¹*Politecnico di Milano (MI), DEIB (Italy)*

²*University of Florence (FI), DINFO (Italy)*

³*LENS and CNR, (FI), INO (Italy)*

Abstract

Feasibility of Topological Metawaveguides supporting helical propagation in the microwave range has been recently proven. The advantages of unidirectional propagation supported by such waveguides however can only be exploited in real devices if topological modes are endowed with the capability to interact within themselves as well as with trivial modes. Here we show a modal launcher to interface a topological metawaveguide with conventional circular waveguides with negligible reflection and we exploit the properties of coupled topological modes to show a proof of concept of a topological contra-directional coupler.

PACS numbers: 78.67.Pt, 41.20.Jb, 42.70.Qs, 84.40.Dc

Keywords: Microwave Topological Insulators, Coupled Topological Modes, Integrated Photonics

In recent years a new field of physics, known as *topological photonics*, has rapidly emerged¹⁻¹¹. Although its initial aim was to emulate, employing highly controllable photonic systems, topological effects originally discovered in quantum matter¹²⁻¹⁴, soon enough Photonic Topological Insulators (PTIs) appeared as an exciting platform for the realization of new robust and low-loss photonic devices. As for condensed matter, PTIs are *insulating* in the sense that they have a complete Photonic Band Gap (PBG) inhibiting traveling bulk photonic states. However their topologically non-trivial order, marked by indexes as Chern or winding numbers^{15,16}, endows their edges with fascinating properties. Although these edge properties emulate their condensed matter counterparts, the flexibility in the design of artificial photonic media^{17,18} also allows to observe phenomena that cannot be easily observed or do not at all have solid-state analogues^{19,20}.

Possibly the most important property of PTI edges is that interfaces between two PTIs, or between a PTI and a non-topological photonic insulator, support gapless unidirectional modes across the common PBG, also called Topologically Protected Edge Modes (TPEMs). Because of the waveguiding features being related to the topology of the confining mirrors, these interfaces are often named Topologically Protected Meta Waveguides (TPMWs). Whereas topological characteristics are invariant under homeomorphic transformations, TPMWs have remarkably robust waveguiding properties even against imperfections of the confining PTIs^{1,2}. The synergy between their robustness and the exceptional feature of unidirectionality makes them promising for a broad range of applications in integrated photonics and nano optics^{7,8}. Reflection-less and unidirectional propagation around disordered regions⁴, sharp bends⁷, and large defects²¹ has been shown both theoretically and experimentally employing different kind of TPMWs.

However, when it comes to real devices, the thrilling robustness of topological modes is rather quickly converted into a double-edged weapon. Indeed even simple applications, as energy conveyance, require some degree of interaction, for instance with a source and a detector, yet topological modes hardly interact with anything else. Therefore, if topological propagation has to be exploited in real world devices, there are two gaps to overcome. On one side one needs to efficiently convert a non-topological mode into a topological one. This includes both being able to excite a topological mode with a non-topological source, and extract power flowing in a topological mode to detect it with a conventional detector, both with minimum losses in the process. On the other side an all-topological platform for signal

processing is desirable, but a fundamental step towards its implementation is the study of interactions between different topological modes.

In this contribution we address both the aforementioned problems using a similar approach based on local breaking of Topological Protection (TP). First we are able to observe an excellent transition between a conventional mode and a topological one by carefully designing a transition region and later applying optimization methods derived from microwave engineering. The designed interface can be used both for an efficient excitation of topological modes, for which we observe a reflection coefficient as low as -10db over the whole bandwidth, and for a full-vectorial detection and characterization of power flowing through a topological channel employing, for instance, S-parameters which are directly measurable from commercial VNAs. On the other hand we qualitatively study the interaction between counterpropagating topological modes. We observe that a local breaking of topological protection results in non-null coupling between counter propagating topological modes which can be used to realize directional and contra-directional couplers. Finally we show a proof of concept for such a *Topological Directional Coupler*

Topological Properties

PTIs have been realized with a large number of micro and nanophotonic platforms. As a general classification one can define two types of systems. First, topological systems supporting chiral unidirectional edge modes, characterized by a \mathbb{Z} topological invariant that counts the number of unidirectional modes across a given bandgap. These systems can be realized by explicitly breaking time-reversal symmetry either using ferromagnetic materials^{1,2} or exploiting Floquet physics^{5,22,23}. Second, topological systems supporting uncoupled counter-propagating topological modes, characterized by a $\mathbb{Z} + \mathbb{Z}$ topological invariant and that can be realized also in presence of time-reversal symmetry^{4,7,24,25}. Very recent researches also demonstrated \mathbb{Z}_2 topological systems in which Floquet temporal modulation enables time-reversal symmetric systems with counter-propagating modes persisting even after inter-spin coupling²⁶. However uncoupled counter propagating modes are attractive *per se* since reflectionless propagation can be observed without any magnetic bias or temporal modulation, yet light propagation direction is usually entangled with some additional property of the EM field (such as polarization) which is interesting for applications as polarization discrimina-

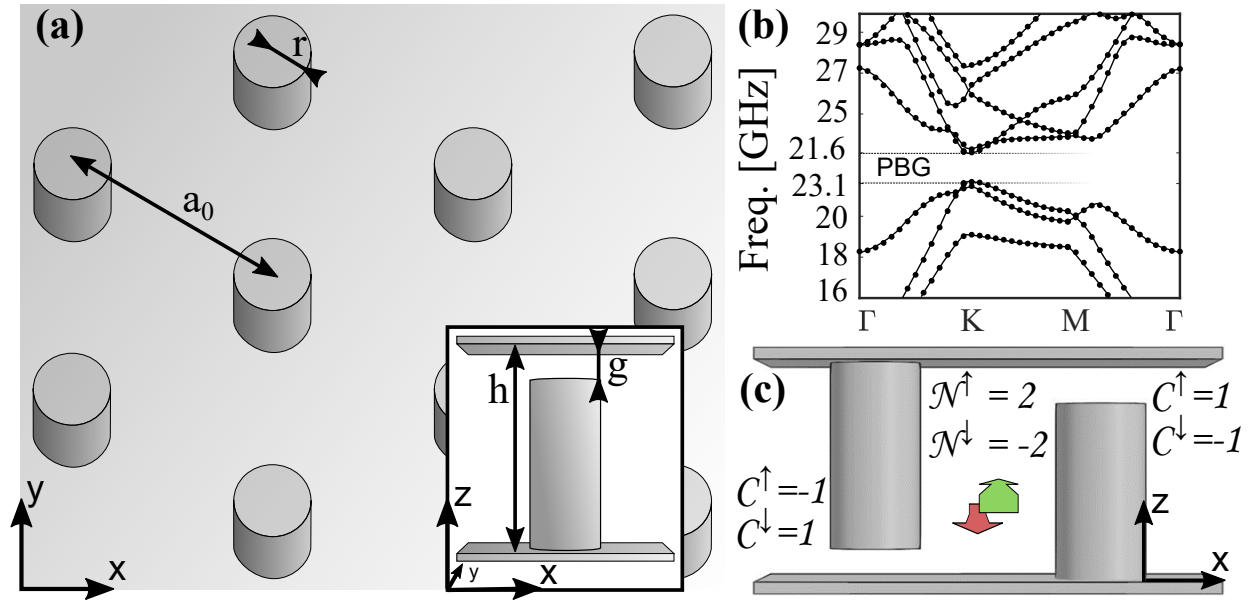


Fig. 1. (a) Schematic of TPhC, $a_0 = 10\text{mm}$, $r = 1.725a_0$, $g = 0.15a_0$, $h = a_0$. (b) Photonic Band Structure (PBS) of the TPhC with the complete PBG highlighted. (c) Topological interface between two z -symmetry reversed TPhCs. The number of unidirectional edge modes for every spin state is given by the difference between the confining spin-Chern Numbers.

tors. Among all existing proposals we base our results upon the bianisotropic metawaveguide concept theoretically introduced in and experimentally demonstrated in⁸, because of its convenient operating frequency range and relatively easy implementation.

The PTI (shown in Fig. 1a) consists in a triangular arrangement of metallic rods, asymmetrically perturbed along the z direction as to introduce an air-gap between the bed-of-rods and one of the confining metallic planes. The eigenfrequencies of the PTI (reported in Fig. 1b) have a complete PBG of $\approx 1.5\text{GHz}$ centered around 22.33GHz . Considering Circular Polarization (CP) basis to express the fields, the four modes, two on the upper and two on the lower edge of the PBG, can be expressed in terms of two uncoupled set of two modes each, one with Right Circular Polarization (RCP) and one with Left Circular Polarization (LCP). Because the two sets are uncoupled one can calculate the Chern number of both sets asunder, denoting them as \mathcal{C}^\uparrow and \mathcal{C}^\downarrow . While time reversal symmetry enforces the total Chern number $\mathcal{C} = \mathcal{C}^\uparrow + \mathcal{C}^\downarrow$ to be zero, the spin-Chern numbers $\mathcal{C}^{\uparrow/\downarrow}$ might individually acquire opposite non-zero integer values. In such case the PTI is equivalent to two uncoupled set of \mathbb{Z} -type PTIs with opposite chirality. For the system under study Ma *et al.*¹⁹ calculated

$\mathcal{C}^{\uparrow/\downarrow} = \pm 1$, with the spin-Chern numbers changing sign also as a result of a z-inversion (relocation of the air gap from the top to the bottom edge). As a matter of fact, two copies of the PTI with reversed position of the air gap, placed one close to the other in such a way that the hexagonal symmetry still holds globally, give rise to a topological domain wall across which the spin-Chern invariants of the structure changes from ± 1 to ∓ 1 . An interface between media with different topological invariants supports a number of edge modes that is equal to the difference between the topological indexes (a fundamental principle known as Bulk-Edge Correspondance). Thereof two ψ^{\uparrow} unidirectional modes are expected as a result of the \mathcal{C}^{\uparrow} difference as well as two ψ^{\downarrow} modes associated to the \mathcal{C}^{\downarrow} difference. These two sets of modes are referred to as *quasi-spin* modes^{7,24,25,27}; they carry energy in opposite directions and, as long as topological protection is maintained, they cannot scatter one into the other. Since the propagation direction of such topological modes is locked with their polarization state it is also common to name them Topologically Protected Helical Edge Mode (TPHEM). We note here that $\mathbb{Z} + \mathbb{Z}$ topological systems supporting TPHEM are different from fermionic systems with Spin-Orbit coupling exhibiting \mathbb{Z}_2 topological insulating phase. In the latter case gap-less topological edge modes are preserved even in the presence of inter-spin coupling (Rashba coupling) while in $\mathbb{Z} + \mathbb{Z}$ PTIs topological protection has to be assisted by additional symmetries. However, as it will be clear in the following, the somehow reduced protection of $\mathbb{Z} + \mathbb{Z}$ insulators is an enabling feature to obtain the exotic coupling features that will be described in the second section of this work.

I. CIRCULAR WAVEGUIDE LAUNCHER

The propagating mode of the structure within a given bandwidth can be excited by an antenna inserted in the TPMW itself. If an antenna with Linear Polarization (LP) is used, the whole set of propagating modes are simultaneously excited leading to four modes, bidirectional, propagation. A more interesting situation is that of an antenna that matches the specific time evolution of the only forward (backward) modes; in the latter case only one kind of pseudo-spin will couple to the excitation, resulting in dual mode, unidirectional propagation. In the initial theoretical proposal⁷ a source with LCP, rotating in the plane containing the structure, has been used to simulate unidirectional excitation. However point dipoles are ideal sources and, while acceptable approximations of ideal dipoles can be

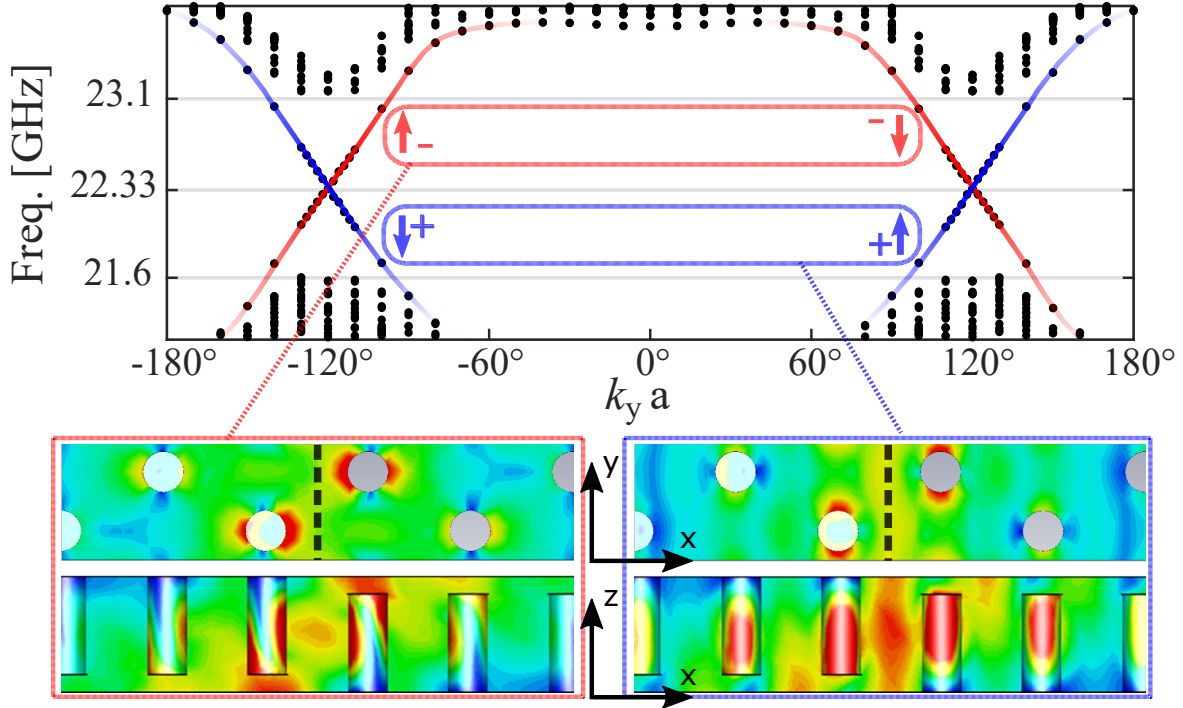


Fig. 2. (color online) **Top:** PBS of the topological interface. Arrows are spin states and signs are modal effective index sign. **Bottom:** Electric field amplitude in the longitudinal and transverse direction for the TPHEMs. The spin state is determined by the time evolution of the electric field in the air gap region.

built, it is unpractical, if not nearly impossible, to build such sources inside the structure. Indeed in the first experimental work⁸ a short dipole antenna has been used for a broadband excitation of the structure by inserting it into the TPMW through a small hole. Although a short dipole is a more practical antenna it is not circularly polarized, therefore both Forward and Backward modes are excited with this scheme. We also note that previous attempts to excite topological modes have not considered the characteristic impedance of the topological modes. Indeed if the antenna is not properly matched to the mode's impedance only a fraction of the feeding power will couple to the travelling mode, being the most part of it reflected towards the power source. If in early experiments this does not represent an issue, it becomes of the uttermost importance if TPMWs shall be used as a component in real life devices.

In this section we propose a design for a modal launcher based on a Circular WaveGuide (CWG). We show how impedance matching can be effectively used to optimize such tran-

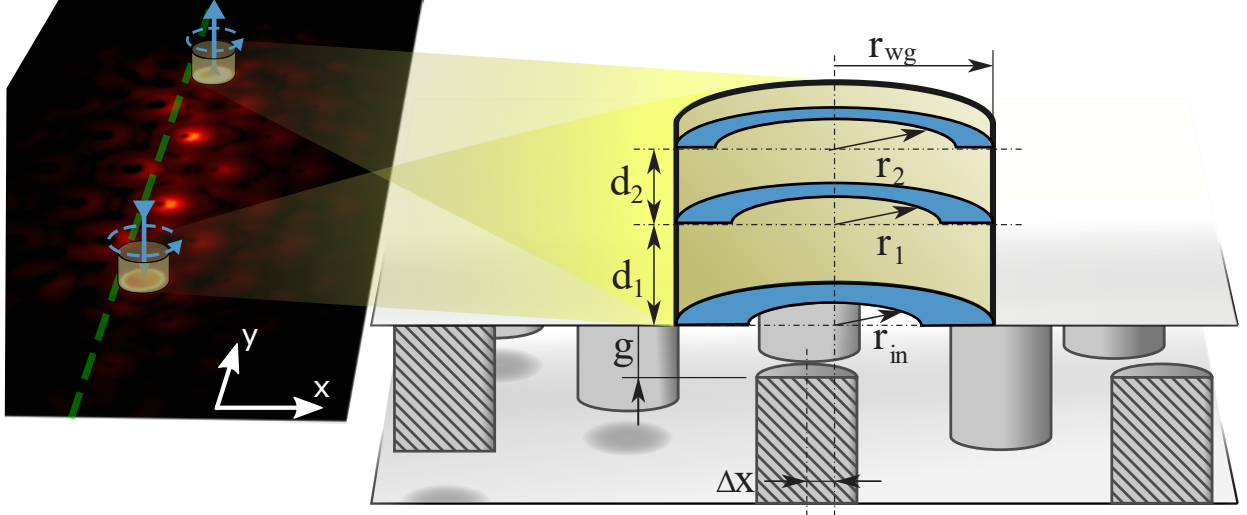


Fig. 3. (color online) **left:** Absolute value of the Poynting vector for a TPHEM propagating from a CWG launcher to a second one placed at a distance of $9a_0$. **right:** Schematic of the CWG launcher.

sition over a relatively large bandwidth thus obtaining low loss excitation of helical modes both for injection and extraction of a test signal. In spite of its simplicity, our approach is easily generalized for any antenna geometry, such as planar or slot antennas²⁸. The low-loss transitions obtained with established optimization methods from microwave engineering provide a way to fully characterize transmission of any kind of TP based microwave device.

a. Design of the launcher: Our design is based on the degenerate $TE_{11}^{x,y}$ modes supported by a CWG. These orthogonal, LP, modes can be easily transformed into a couple of CP clockwise and anti-clockwise modes by a transformation matrix.

$$\mathbf{T} = \frac{1}{\sqrt{2}} \begin{bmatrix} 1 & j \\ 1 & -j \end{bmatrix} \quad (1)$$

A circular hole cut in the top metal plate of the TPMW can be used to couple a $-z$ directed CWG to the topological structure with an excellent matching of the TPHEMs's pseudo-spin. The radius of the CWG is a fixed design constant and is chosen in order to have only first order modes propagating. After fixing the CWG radius the design of the modal launcher is carried out in two distinct steps. At first we consider the transition itself, whose frequency response strongly depends on the coupling hole position and radius and subsequently we optimize the coupling with the CWG in order to minimize reflections.

Due to the underlying hexagonal symmetry of the lattice we expect an asymmetric behaviour of the transition with respect to the two LP modes of the CWG. This might give rise to a cross-polarization term across the transition which causes an incident L(R)CP waveguide mode to excite a fraction of R(L)CP mode in the TPMW. Eventually this will result to radiation in the undesired direction and unwanted losses; the goal of the first step is minimizing this source of losses. We also observe that purest CP of the topological mode is located in a point $\Delta x \approx 0.65r$ away from the interface starting from the rod's center. Using that point as the excitation axis, we vary the hole radius and calculate the pointing vector flux across both ends of the waveguide, P_{fw} and P_{bw} . Having defined the ratio $\eta = P_{\text{fw}}/(P_{\text{fw}} + P_{\text{bw}})$ as a figure of merit for the effectiveness of the Forward (Fw) excitation, we find a maximum of η for $r_{\text{in}}/r = 2.25$ (see Fig. 4a).

To optimize the coupling to the CWG we first obtain the frequency dependent S-parameters matrix relative to the LP waveguide modes (\mathbf{S}^L) from the de-embedded input impedances of the optimized window. A congruent transformation can be used to transform the S-parameters to a basis of CP modes^{29,30}

$$\mathbf{S}^C = \mathbf{T}^* \mathbf{S}^L \mathbf{T}^\dagger \quad (2)$$

Where the \mathbf{T} matrix is given in (1). Note that the simple conjugate in the first term of the RHS in (2) inverts the rotation direction of R(L)CP modes for the reflected (outgoing) waves and is required in order to maintain the symmetry of the transformed \mathbf{S}^C matrix³⁰. The diagonal terms of the \mathbf{S}^C matrix, related to a cross-polarization reflection and given by $S_{l(r),l(r)} = (S_{x,x}^L - S_{y,y}^L)/2 \pm iS_{x,y}^L$ can be used as a first approximation for evaluating the asymmetry of the transition. For the optimized window this term is smaller than 20dB over the entire topological bandwidth, this confirms that the S-parameters for the orthogonal LP modes are approximately equal to each other and that the CWG coupling can be optimized using axisymmetric elements, having the same effect on both LP modes. The cascade of a CWG with the above mentioned window can be represented as a transmission line with a characteristic impedance given by the generalized impedance of the first order CWG modes, connected to a frequency-dependent load with impedance given by the input impedances window itself. In such a configuration an incident wave will exhibit a reflection on the load given by (3)

$$\Gamma = \frac{Z_L - Z_0}{Z_L + Z_0} \quad (3)$$

Where Z_L is the load impedance and Z_0 is the transmission line characteristic impedance. Load matching is the procedure of using a matching network, placed between the load and the transmission line, in order to modify the equivalent load impedance with the goal of matching the transmission line's characteristic impedance and eliminate reflections³¹. For narrow band operation the procedure is easily performed in a deterministic way by first moving, along the transmission line, to a distance from the load in which its normalized impedance Z_L/Z_0 has unitary real part, and then eliminating the residual reactance by placing an element with purely imaginary opposite reactance in parallel to the load. Broadband operation, conversely, involves multi-stage matching with a high number of degrees of freedom which generally requires a numerical optimization strategy. In the present case, inductive irises can be used for realizing purely imaginary loads. The degrees of freedom for the design of a double irises matching circuit are illustrated in Fig. 3. In addition, the irises' thickness has also been parametrized in order to fine tune the matching network response.

The optimization is performed with a genetic algorithm^{32,33} in which the response of the matching circuit is simulated with the Mode Matching method³⁴. In the end of the optimization routine we obtain a reflection coefficient lower than -10dB over a bandwidth of 1.1GHz with peaks of -20dB, using irises with thickness $t = 0.5\text{mm}$, distances $d_1 = 6.75\text{mm}$, $d_2 = 7.65\text{mm}$ and radii $r_1 = 0.62r_{\text{wg}}$, $r_2 = 0.66r_{\text{wg}}$ (see Fig. 4b).

The matching bandwidth, calculated as the spectral region with reflection coefficient lower than -10dB, covers $\approx 73\%$ of the bulk PBG. That is sufficient to characterize with S-parameters typical features of topological propagation, such as reflection-less propagation of polarization-locked waves around sharp bends across all the bulk PBG.

b. Probing topological protection: As previously said, rotating sources matched to the quasi-spin temporal evolution as the one considered in this and previous works^{7,35}, can be employed to select a specific quasi-spin degree of freedom but not to excite a single propagating mode. Indeed both positive and negative effective indexes Fw modes are excited in response to a LCP input, with arbitrary amplitude-phase relation that is typical for every specific launcher design. Since the effective load of the TPMW is strongly dependent on the excited fields, the transition will behave as expected only at those points in which the amplitude-phase relation of the propagating modes is equal to the one at the excitation point. These points of the TPMW are the only ones in which an output interface is able to efficiently convert a TPHEM to a conventional waveguide mode and are identified as

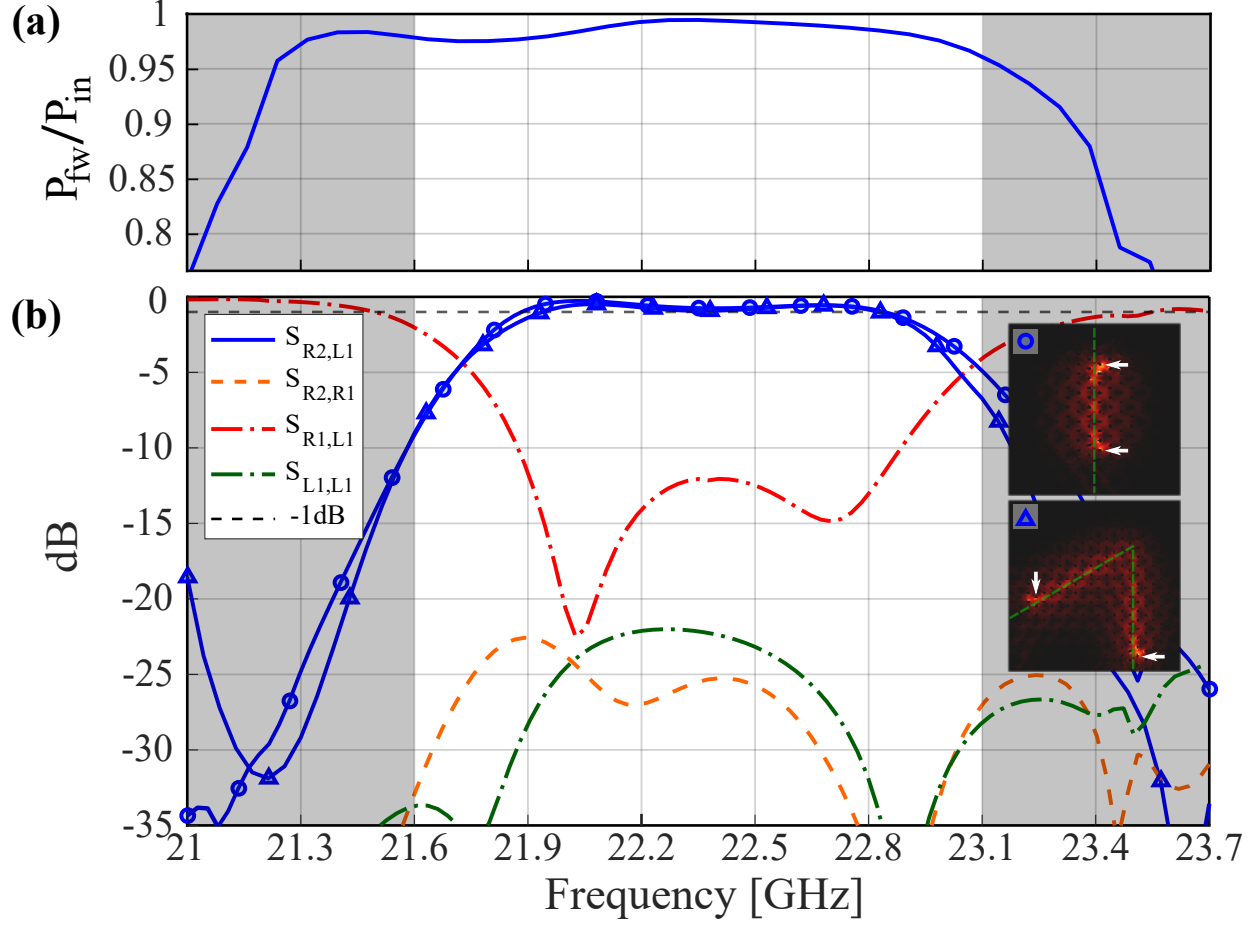


Fig. 4. (color online) (a) Ratio between Fw and total outgoing power as a function of excitation frequency. (b) *Solid lines*: LCP-to-RCP transmission of the straight (circles) and bent (triangles) TPMWs. *Dash-point*: Single port co and cross polarization reflection coefficients. *Short dash*: RCP-to-RCP transmission of the straight TPMW. *Inset*: Poynting vector at $z = h/2$; TPMW is indicated with green short-dash line while white arrows indicate CWG launchers positions.

extraction points. The distance between an excitation point and an extraction point, or between two possible extraction points is given by the beating length of the two propagating modes, which is in turn determined by the difference in the TPHEM propagation constants, $\Delta_{\pm} = k_{+} - k_{-} = 4\pi/3a_0$. Luckily enough Δ_{\pm} turns out to be approximately constant across all the PBG so that the interference period P_y along the propagation direction is also constant and can be calculated as the (integer) number of reticular constants required to obtain a phase difference of $\Delta\phi = 2\ell\pi = \Delta_{\pm}P_y$. Since P_y/a_0 must be an integer, setting $\ell = 2$ one obtains $P_y = 4\pi/\Delta_{\pm} = 3a_0$. This super-reticular periodicity can be observed in

Fig. 3 and it enforces the distance $L_{i/o}$ between an input and an output port to always be $L_{i/o} = mP_y = 3ma_0$, with m integer.

In order to demonstrate the effectiveness of the proposed launcher in characterizing topological propagation we model a straight TPMW and a bent one, with a very sharp deg 120 turn. We place input and output interfaces at appropriate distances and measure the scattering parameters between the two ports. While an RCP input is attenuated more than 20 dB before exiting from the output port, an LCP input is transmitted with maximum total losses of 1dB over a fractional bandwidth of 4.4% which represents the 64% of the PBG; transmission with maximum total losses of 3dB is instead observed over 87% of the PBG. Moreover, the transmission spectra of the straight and bent TPMWs are nearly equal inside the matching bandwidth, which confirms the topological nature of TPHEMs propagation.

As a final note we stress out that input and output coupling happens through out-of plane propagation, and thus propagation direction is inverted for an input and an output wave. Although an input LCP mode on port 1, rotating in the counter-clockwise direction, is coupled to Ψ^\uparrow modes flowing in the Fw direction, the corresponding transmitted mode in the output port 2 is still rotating in the counter-clockwise direction but is defined, accordingly to (2), as an outgoing RCP. Only with these definitions is the reciprocity of the structure conserved since an incoming RCP wave on port 2 is now reciprocally coupled to a Ψ^\downarrow Backward (Bw) mode and transmitted to the LCP output at port 1.

II. COUPLED TOPOLOGICAL MODES

In the second part of this paper we focus on the interaction between different topological modes, coupling through evanescent fields. Topological modes are not expected to show strong evanescent coupling, indeed one of the requirements for topological protection is the complete absence of coupling between different modes. However perturbations play a huge role in this case; it is possible to devise regions in which topological protection is broken, and use these regions to obtain some degree of interaction between topological modes. We study in a qualitative way the interactions between closely placed bianisotropic TPMW, in a structure that we call Coupled Topologically Protected Meta Waveguides (CTPMW). We show that they exhibit peculiar coupling effects with a strong spectral dependence which we explain as the interplay of two different coupling phenomena namely *spin* and *inter-*

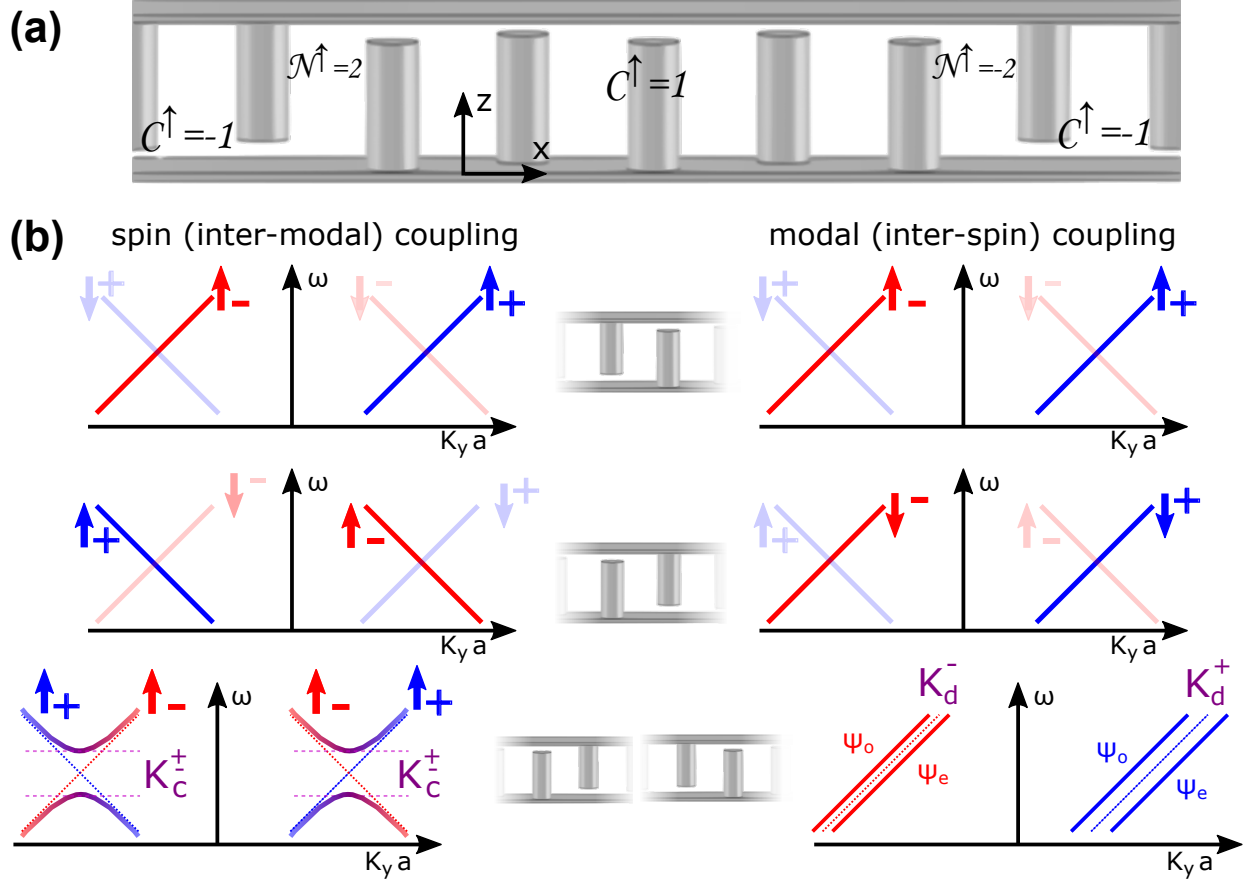


Fig. 5. (color online) (a) Double topological interface with $N = 5$ interstitial rods. *Spin up* modes have different propagation directions in the two TPMWs (b) *left*: Ψ^\uparrow eigenmodes of the left interface couple to Ψ^\uparrow eigenmodes of the right interface when phased matched, causing anti-crossing. *right*: Ψ^\uparrow modes of the left interface couple to Ψ^\downarrow modes of the right interface across all the PBG causing symmetric/anti-symmetric pair splitting.

spin coupling. Eventually we summarize our findings by illustrating a proof-of-concept of a directional coupler for topological states.

Dual symmetric interface

Figure 5a shows the cross section of a dual symmetric interface that can be obtained by sandwiching a number N_s of up-facing rods between two bulk crystals of down-facing rods. Recalling that $C^{\uparrow/\downarrow}$ reverses its sign at any relocation of the air gap, because of the Bulk-Edge Correspondence principle the two TPMWs needs to have inverted handedness. Moreover

the CTPMW structure is symmetric along the x axis as opposed to the uncoupled TPMW; as a consequence the modes of the right interface in Fig. 5a are exactly the same modes of the left interface, apart from a change in the sign of the wave vector k_y and propagation direction. A complete and rigorous coupled mode formulation for the problem would require to take the interplay between all four modes of the two TPMWs into account, leading to 16 coupled mode equations. However, the problem can be dramatically simplified by neglecting couplings between different modes of the same TPMW because of their orthogonality in the uncoupled case, and dividing the inter-TPMW couplings into only two distinct phenomena: *Spin* couplings and *inter-spin* couplings. These two phenomena are schematically depicted in the left and right sides respectively of Fig. 5b and will be illustrated in the following.

a. Spin (inter-modal) coupling: The dispersion relation of an uncoupled TPMW (Fig. 2) shows two degeneracy points ($k = \pm 120^\circ$ at $f = 22.33\text{GHz}$) between Ψ^\uparrow and Ψ^\downarrow modes. These modal intersections are protected by spin-orthogonality condition meaning that counter-propagating modes belong to uncoupled spin subspaces thus cannot give rise to anticrossing. In the dual symmetric case, however, counter-propagating modes of different waveguides belongs to the same spin subspace (because of the inverted guides handedness) and coupling is not prohibited. Since spin-coupling involves interaction between n_{eff}^\pm and n_{eff}^\mp modes, but with the same spin, it can also be referred to as an *inter-modal* coupling; it is mediated by the phase matching condition and as such will be present only in a small frequency range, ultimately resulting in avoided crossing that opens a small gap in the interfaces' dispersion. A straightforward consequence of the described spin coupling mechanism is that a Fw mode traveling in one of the two CTPMWs will progressively leak its energy to a Bw mode of the other TPMW, a phenomenon known as Contra-Directional coupling³⁵. While in conventional Contra-Directional (CD) couplers the required phase matching between Fw and Bw modes is satisfied by an appropriately designed Bragg grating between the two waveguides, it is automatically present in our CTPMWs structure because of the modes symmetries. As it will be further discussed in the following, Topological CD coupling offers several advantages with respect to conventional Bragg-assisted one.

b. Inter-spin (modal) coupling Away from the degeneration frequency spin-coupling cannot happen because of phase matching not being satisfied. At the same time spin-orthogonality seemingly prevents coupling of modes with opposite spin thus preventing any kind of coupling in the CTPMW structure. However, topological order is partially lost in

the central region because of the mutual perturbation between the two TPMWs and the finite size of the central domain. This breaks the orthogonality between spin-reversed (and co-directional) modes of the two waveguides, which can interact. In this regime the coupling is weak, even if the CTPMWs are close, because power transfer from one TPMW to the other involves a change of spin (thus polarization). The coupling length L_0 is expected to be several reticular constants long and, in principle, different between positive and negative index modes because of their different degrees of edge localization.

The simultaneous effects of both coupling mechanisms can be observed looking at the modes of an infinite strip comprising both CTPMWs (Fig. 6). Every mode of the uncoupled TPMW divides into a couple of symmetric/antisymmetric modes (also called super-modes), confirming that there is directional coupling between the two CTPMWs. Indeed the difference between the super-modes' propagation constants ($\beta_s - \beta_a = \Delta_{sa} \neq 0$) gives rise to a coupling length L_0 , defined at each frequency as half the beating length of the modes: $L_0 = \pi/\Delta_{sa}$ ³⁶. At the same time anti crossing happens around the degeneration frequency with a bandwidth related to the coupling strength (Fig. 7a). To confirm that the modes couples (whose dispersion is depicted in the main Fig. 6) are symmetric-antisymmetric pairs we look at their even and odd recombinations and retrieve field profiles compatible with the uncoupled TPHEMs (Fig. 6 inset).

Hybrid D/CD coupler

As a proof of concept for the behavior of the CTPMW structure we now show an hybrid Directional/CD coupler that acts on topological states. One of the most critical points in conventional directional couplers is the design of the input/output tapering sections. In these regions two waveguides are bent in order to bring them close together down to a minimum distance in which the mutual interaction between the two is sufficiently strong. These bends normally introduce non-negligible losses that can only be addressed by increasing the curvature radius and, consequently, device sizes. A topological directional coupler is, on the contrary, immune to these losses and as such it provides a straightforward way to decrease the footprint of photonic devices that are based on a high number of directional couplers. Furthermore, the unique features of the CTPMWs allow for the design of a device which is at the same time a Directional and a Contra-Directional coupler, depending on the input

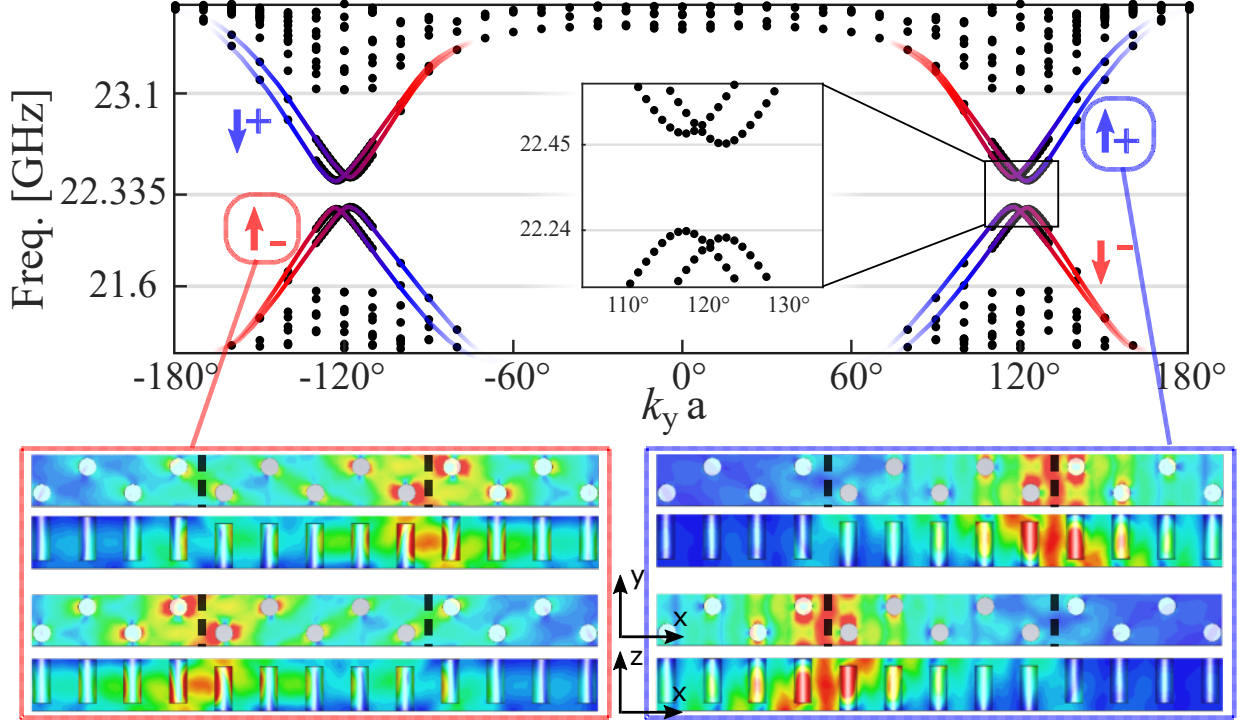


Fig. 6. (color online) PBS of the double interface. **Inset:** longitudinal and transverse electric field amplitudes for evenly (top) and oddly (bottom) combined eigenmodes couples.

frequency, providing rich spectral features.

The basic structure of our topological directional coupler is illustrated in Fig. 7b in which the input/output sections are clearly visible together with the interaction section. Our design depends on 2 parameters: The inter-waveguide separation N_s that controls the relative bandwidth of the contra-directional region (see Fig. 7a) and the interaction length L_c that controls the splitting ratio in directional coupling regime. In our numerical simulations the uncoupled TPMWs eigenmodes have been used as input and output, but every other kind of excitation can be used, including the previously discussed CWG launcher.

When exciting the input port for frequencies outside of the secondary gap, the propagating field on the input TPMW overlaps with an even superposition of both CTPMW supermodes $\psi_1 = 1/2(\psi_s + \psi_a)$. After propagating for a coupling length L_0 the two supermodes acquire a π phase shift, producing a field completely localized at the second interface ($\psi_2 = 1/2(\psi_s - \psi_a)$). In this regime the device behaves as an optical directional coupler where the length of the interaction section defines the splitting ratio $\eta_s = P_{\text{cross}}/(P_{\text{cross}} + P_{\text{bar}})$. For

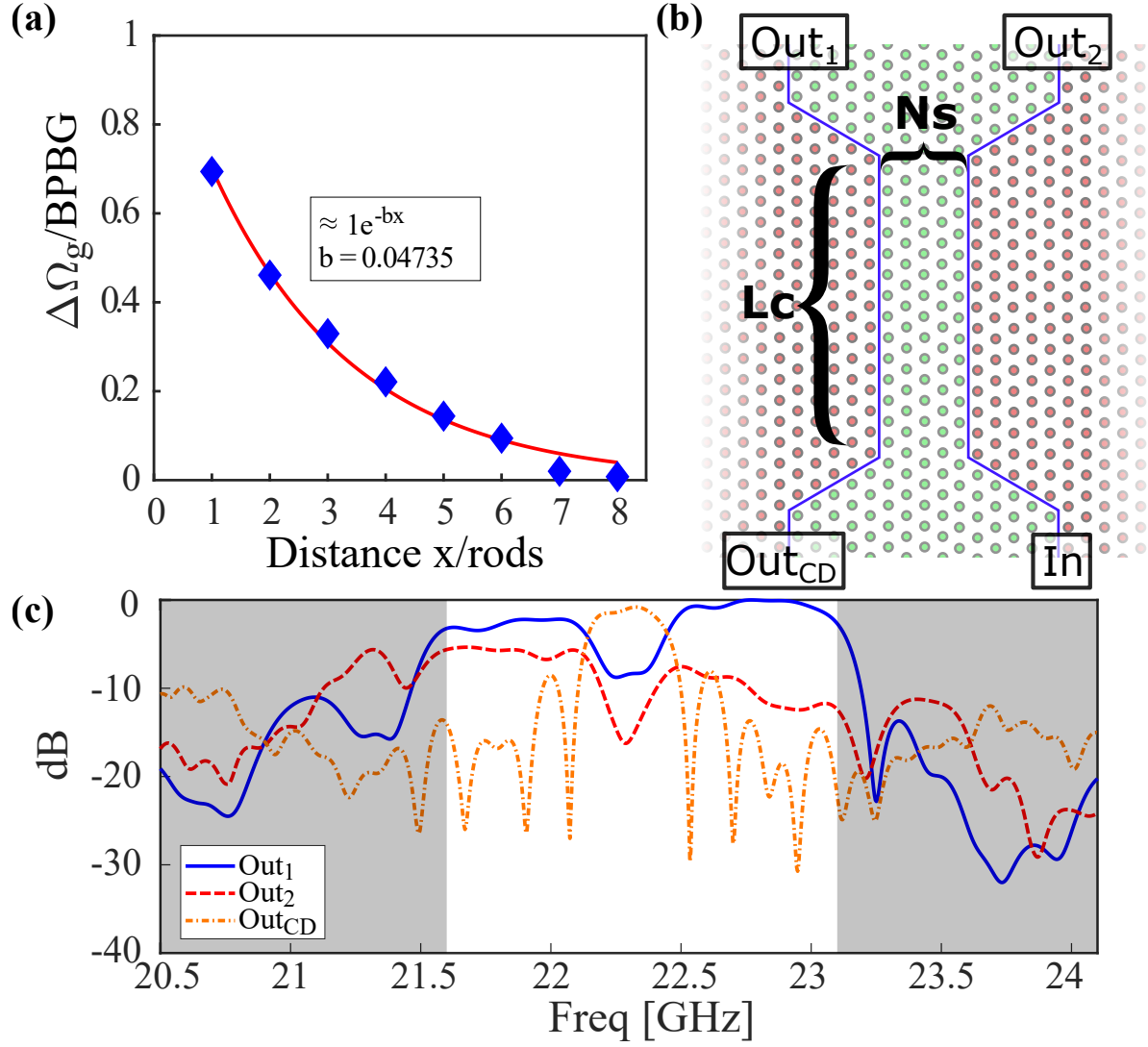


Fig. 7. (color online) (a) Normalized bandwidth of the secondary frequency gap as a function of inter-guide separation. TPMWs. (b) Directional Coupler Structure: Red and green dots represent rods with the air gap in opposite position. Blue lines indicates TPMWs. (c) Transmission spectra for a coupler with $L_c = 30$ and $N_s = 5$.

frequencies belonging to the anticrossing bandwidth, on the contrary, there are no allowed propagating states in the CTPMWs. An input wave should be back-reflected towards the source but, as previously anticipated, this is forbidden by spin conservation and the only path that can be followed by the propagating wave is to couple to the phase matched Bw mode of the coupled TPMW. In this regime the coupling Contra-Directional, the transmittance peak of the CD coupling rapidly approaches 1 with increasing coupling section length L_c ,

meaning that the coupling is fairly strong, while the bandwidth of the CD effect is only influenced by the separation between the two waveguides and exponentially decreases for increasing distances.

CD coupling is a well-known phenomenon in literature^{37,38} and it is normally achieved by using Bragg gratings³⁹. Interestingly enough however, because of the symmetries that defines spin states, CD coupling appears as the predominant coupling phenomenon in QSH-like PTIs. Topological CD coupling happens without the need of designing an appropriate Bragg grating and, if the coupling is strong enough, it can be present on a very large portion of the TPMW operating bandwidth (see Fig. 7a). Moreover, spin orthogonality for the uncoupled TPMW impairs self back-coupling, a phenomenon for which the input Fw mode is coupled to a Bw mode of the same waveguide rather than a Bw mode of the coupled waveguide. In conventional Bragg-assisted CD couplers this unwanted phenomenon is addressed by introducing a detuning between the two coupled waveguides, which in turn has detrimental effects in the co-directional coupling regime. Conversely, spin conservation allows for a perfectly balanced design which conserves the device functionality also in the Directional coupling regime.

A coupling section length of $30a_0$ and a guide separation of $N_s = 5$ rods produces a device with a $\approx 50\%$ splitting ratio for $f < 22.1\text{GHz}$, a complete cross state for $f > 22.5\text{GHz}$ and almost unitary contra-directional coupling transmission for $f \in [22.1, 22.5]\text{GHz}$ (Fig. 7c). The described hybrid directional/CD coupler is simulated through Full-Wave simulations on CST MWS with matched impedance boundary condition in order to eliminate reflections on the boundaries. To obtain the transmission diagram of Fig. 7c we define 6 field probes along the TPMW interface, close to each device port, with a relative distance of $a_0/2$. Then we extract the frequency dependent field intensity at each port by mediating the field intensities recorded by each of the 6 field probes in order to smooth the interference pattern as described in⁸. Finally the transmittance at any physical port is defined as the ratio of the port field intensity and the field intensity measured at the input port.

CONCLUSIONS

We illustrated how load matching procedure can be applied to design a modal launcher for topological modes. Our optimized circular waveguide transition has a relative matching

bandwidth of $\approx 73\%$ with respect to the operating bandwidth of the Topologically Protected Meta Waveguide and it can be used to directly probe topological protection, by observing broadband perfect transmission around a very sharp bend of the topological waveguide.

We studied the coupling mechanisms of two interacting TPMWs by illustrating *spin (inter modal)* coupling and *inter-spin (modal)* coupling. These happen in distinct spectral regions and give rise to different coupling phenomena, respectively Contra-Directional and Directional coupling. Finally we presented a simple design for a device that implements a topological Directional-Contra Directional coupler. Our proposed design can be used to route a topological mode through three output ports and can be used to realize devices as beam splitters, interferometers and routers based entirely on topological propagation. Topological protection also makes the device less affected by the bends introduced by the tapered sections and keeps the design robust with respect to a class of fabrication defects (in particular missing or misplaced rods). The topological Directional Coupler might also find applications in testing Topological Photonics to the quantum regime since a 50% beam splitter is often mandatory in many quantum optics experiments.

* piccioli@lens.unifi.it

¹ Z. Wang, Y. Chong, J. D. Joannopoulos, and M. Soljačić, Physical Review Letters **100** (2008).

² Z. Wang, Y. Chong, J. D. Joannopoulos, and M. Soljačić, Nature **461**, 772 (2009).

³ F. D. M. Haldane and S. Raghu, Physical Review Letters **100** (2008), 10.1103/PhysRevLett.100.013904.

⁴ A. B. Khanikaev, S. Hossein Mousavi, W. K. Tse, M. Kargarian, A. H. MacDonald, and G. Shvets, Nature Materials **12**, 233 (2013).

⁵ M. C. Rechtsman, J. M. Zeuner, Y. Plotnik, Y. Lumer, D. Podolsky, F. Dreisow, S. Nolte, M. Segev, and A. Szameit, Nature **496**, 196 (2013).

⁶ L. Lu, J. D. Joannopoulos, and M. Soljačić, Nature Photonics **8**, 821 (2014).

⁷ T. Ma, A. B. Khanikaev, S. H. Mousavi, and G. Shvets, Physical Review Letters **114** (2015), 10.1103/PhysRevLett.114.127401.

⁸ K. Lai, T. Ma, X. Bo, S. Anlage, and G. Shvets, Scientific Reports **6** (2016), 10.1038/srep28453.

⁹ M. C. Rechtsman, Y. Lumer, Y. Plotnik, A. Perez-Leija, A. Szameit, and M. Segev, 2016

- Progress in Electromagnetic Research Symposium (PIERS) **3**, 974 (2016).
- ¹⁰ A. B. Khanikaev and G. Shvets, *Nature Photonics* **11**, 763 (2017).
- ¹¹ T. Ozawa, H. M. Price, A. Amo, N. Goldman, M. Hafezi, L. Lu, M. C. Rechtsman, D. Schuster, J. Simon, O. Zilberberg, and I. Carusotto, *Rev. Mod. Phys.* **91**, 015006 (2019).
- ¹² C. L. Kane and E. J. Mele, *Science* **314**, 1692 (2006).
- ¹³ B. A. Bernevig, T. L. Hughes, and S.-C. Zhang, *Science* **314** (2006), 10.1126/science.1133734.
- ¹⁴ M. Z. Hasan and C. L. Kane, *Reviews of Modern Physics* **82**, 3045 (2010).
- ¹⁵ M. S. Rudner, N. H. Lindner, E. Berg, and M. Levin, *Phys. Rev. X* **3**, 031005 (2013).
- ¹⁶ F. Nathan and M. S. Rudner, *New Journal of Physics* **17**, 125014 (2015).
- ¹⁷ J. D. Joannopoulos, *Photonic crystals* (Princeton University Press, 2008).
- ¹⁸ S. Longhi, *Laser & Photonics Reviews* **3**, 243 (2009).
- ¹⁹ T. Ma and G. Shvets, *Physical Review B* **95** (2017), 10.1103/PhysRevB.95.165102.
- ²⁰ A. Quelle, C. Weitenberg, K. Sengstock, and C. M. Smith, *New Journal of Physics* **19**, 113010 (2017).
- ²¹ S. Yves, R. Fleury, T. Berthelot, M. Fink, F. Lemoult, and G. Lerosey, *Nature Communications* **8**, 16023 (2017).
- ²² L. J. Maczewsky, J. M. Zeuner, S. Nolte, and A. Szameit, *Nature Communications* **8** (2017), 10.1038/ncomms13756.
- ²³ S. Mukherjee, A. Spracklen, M. Valiente, E. Andersson, P. Hberg, N. Goldman, and R. R. Thomson, *Nature Communications* **8** (2017), 10.1038/ncomms13918.
- ²⁴ T. Ma and G. Shvets, *New Journal of Physics* **18**, 25012 (2016).
- ²⁵ S. Barik, H. Miyake, W. DeGottardi, E. Waks, and M. Hafezi, *New Journal of Physics* **18**, 113013 (2016).
- ²⁶ L. J. Maczewsky, B. Höckendorf, M. Kremer, T. Biesenthal, M. Heinrich, A. Alvermann, H. Fehske, and A. Szameit, *arXiv e-prints*, arXiv:1812.07930 (2018), arXiv:1812.07930 [physics.optics].
- ²⁷ C. He, X.-C. Sun, X.-P. Liu, M.-H. Lu, Y. Chen, L. Feng, and Y.-F. Chen, *Proceedings of the National Academy of Sciences* **113**, 4924 (2016).
- ²⁸ G. G. Gentili, N. guarducci, G. Pelosi, F. Piccioli, and S. Selleri, in *2019 Progress In Electromagnetics Research Symposium (PIERS)* (Rome (IT), to be presented).
- ²⁹ C. D. Graves, *Proceedings of the IRE* **44**, 248 (1956).

- ³⁰ G. G. Gentili, G. Pelosi, F. Piccioli, and S. Selleri, *Microwave and Optical Technology Letters* **61**, 464 (2019).
- ³¹ S. Selleri, *IEEE Antennas and Propagation Magazine* **53**, 180 (2011).
- ³² E. Agastra, G. Pelosi, S. Selleri, and R. Taddei, “Multiobjective optimization techniques,” in *Wiley Encyclopedia of Electrical and Electronics Engineering* (American Cancer Society, 2014) pp. 1–29.
- ³³ E. Agastra, G. Bellaveglia, L. Lucci, R. Nesti, G. Pelosi, G. Ruggerini, and S. Selleri, *Progress In Electromagnetics Research* **83**, 335 (2008).
- ³⁴ T. Itoh, *Numerical techniques for microwave and millimeter-wave passive structures* (J. Wiley, 1989).
- ³⁵ G. G. Gentili, G. Pelosi, F. Piccioli, and S. Selleri, in *2017 IEEE International Symposium on Antennas and Propagation & USNC/URSI National Radio Science Meeting* (San Diego (CA), 2017) pp. 59–60.
- ³⁶ W. K. Burns, *Journal of Lightwave Technology* **6**, 1051 (1988).
- ³⁷ M. Qiu and M. Swillo, *Photonics and Nanostructures - Fundamentals and Applications* **1**, 23 (2003).
- ³⁸ V. Jandieri, K. Yasumoto, and J. Pistora, *Journal of the Optical Society of America A* **31**, 518 (2014).
- ³⁹ W. Shi, X. Wang, C. Lin, H. Yun, Y. Liu, T. Baehr-Jones, M. Hochberg, N. A. F. Jaeger, and L. Chrostowski, *Optics Express* **21**, 3633 (2013).